


## Motion of Viscous Droplets in Rough Confinement: Paradoxical Lubrication

Ludovic Keiser,<sup>1,2,\*</sup> Armelle Keiser,<sup>1</sup> Manon L'Estimé,<sup>1</sup> José Bico,<sup>1</sup> and Étienne Reyssat<sup>1,†</sup>

<sup>1</sup>Laboratoire de Physique et Mécanique des Milieux Hétérogènes (PMMH), Sorbonne Université, barre Cassan A, 7 quai Saint-Bernard, 75005 Paris, France—CNRS UMR 7636, ESPCI Paris-PSL Research University, Univ. Paris Diderot

<sup>2</sup>Total S.A., Pôle d'Études et de Recherche de Lacq, BP47 64170 Lacq, France

 (Received 11 May 2018; published 19 February 2019)

We study the sedimentation of highly viscous droplets confined inside Hele-Shaw cells with textured walls of controlled topography. In contrast with common observations on superhydrophobic surfaces, roughness tends here to significantly increase viscous friction, thus substantially decreasing the droplets mobility. However, reducing confinement induces a jump in the velocity as droplets can slide on a lubricating layer of the surrounding fluid thicker than the roughness features. We demonstrate that increasing the viscosity of the surrounding liquid may counterintuitively enhance the mobility of a droplet sliding along a rough wall. Similarly, a sharp change of the droplet mobility is observed as the amplitude of the roughness is modified. These results illustrate the nontrivial friction processes at the scale of the roughness, and the coupling between viscous dissipation in the drop, in the front meniscus, and in the lubricating film. They could enable one to specifically control the speed of droplets or capsules in microchannels, based on their rheological properties.

DOI: 10.1103/PhysRevLett.122.074501

Numerous interfacial instabilities induce the emulsification of petroleum in porous media such as snap off [1], viscous fingering [2–4], or pure capillary phenomena [5]. The displacement of the generated droplets in the porous network leads to complex rheology [6]. More generally, the transport of droplets in confined environments is crucial for medical and chemical engineering applications, as illustrated by the fast development of digital microfluidics [7,8]. This problem stimulated numerous studies on the dynamics of confined drops in ideal geometries that demonstrated the major contribution of lubricating films, but remained focused on smooth confining walls [9–17]. In practice however, walls present natural or engineered roughness. Although important works focus on the reduced friction on superhydrophobic surfaces [18–23] and on the reduced adhesion on liquid-infused surfaces of controlled topography [24–26], the impact of roughness on the dynamical properties of the lubricating film has not been extensively studied.

In this Letter, we analyze the sedimentation dynamics of nonwetting oil droplets confined in Hele-Shaw cells filled with a less viscous surfactant solution. By comparing droplets moving in smooth and rough confinements, we highlight the impact of roughness on the mobility of the droplets. Our experimental setup (Fig. 1) is composed of two parallel glass plates covered with a square array of micropillars of square cross section (height  $h$ , width  $w$ , separation  $s$ ) cast in a layer of transparent resin (NOA from Thorlabs) using photolithography techniques (details in the Supplemental Material [27]). The walls are separated by a gap  $e$  ranging from 300 to 1500  $\mu\text{m}$ , much larger than the

micrometric height  $h$  of the textures, as sketched in Fig. 1. The cell is immersed in a bath of a surfactant solution, containing 5% in mass of a commercial soap (PAIC, from Colgate-Palmolive) of dynamic viscosity  $\mu_w = 1 \text{ mPa}\cdot\text{s}$ .

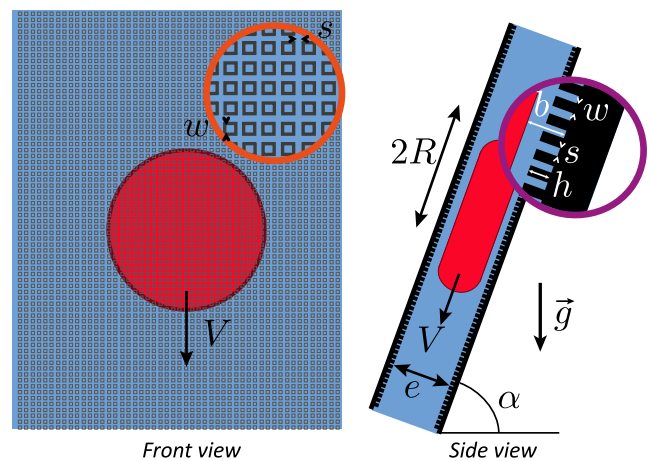


FIG. 1. Experimental setup. A drop of fluorinated oil (red) is confined between the rough walls of a Hele-Shaw cell filled with a surfactant solution (blue). The cell is inclined by an angle  $\alpha$  with respect to the horizontal. The thickness  $e$  of the gap ranges from 300 to 1500  $\mu\text{m}$ . The cell walls are covered with a lattice of micropillars of square cross section of height  $h \ll e$ , width  $w$ , and separation  $s$ . The denser drop (radius  $R$  and volume  $\Omega = \pi R^2 e$ ) falls under gravity with a steady velocity  $V$ . A lubricating film of surfactant solution separates the drop from the walls, with an average thickness  $b$  between the drop and the bottom of the roughness.

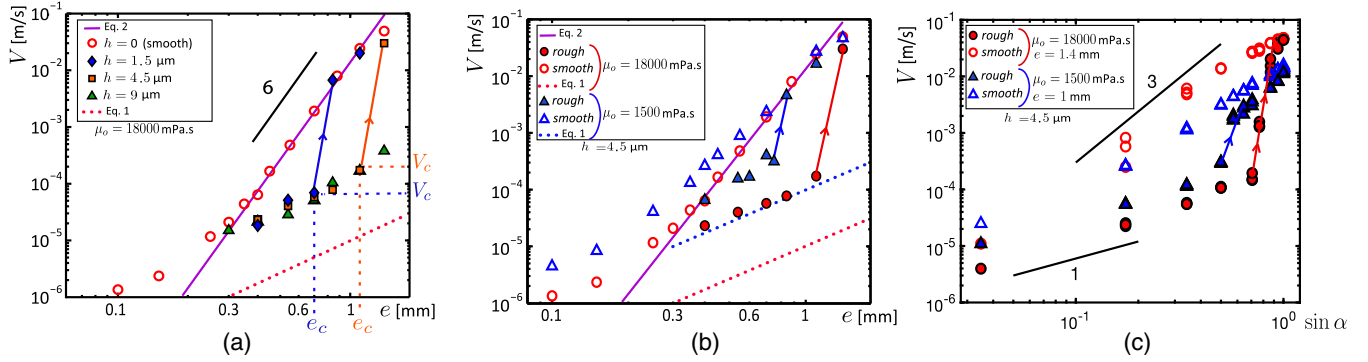


FIG. 2. (a) Falling velocity  $V$  in vertical cells vs the gap  $e$  for different pillar heights  $h$ , for  $\mu_o = 18000$  mPa.s, texture width  $w = 180 \mu\text{m}$  and spacing  $s = 35 \mu\text{m}$ . For smooth walls (empty red circles),  $V$  increases as  $e^6$  [Eq. (2), solid magenta line]. In rough cells and below a critical velocity  $V_c$ ,  $V$  grows as  $e^2$  as expected for a classical Poiseuille flow (dotted red line), but with a significantly higher prefactor, a signature of the slip introduced by the roughness. For  $e > e_c$ , or equivalently  $V > V_c$ , a “jump” of velocity is observed (indicated by arrows and illustrated in the Supplemental Material [27], movie 1) and  $V$  is captured by Eq. (2), as for smooth cells. The critical velocity  $V_c$  increases with the textures height  $h$ , and for  $h = 9 \mu\text{m}$  (green triangles), we do not observe any jump in velocity within the explored gaps. (b) Influence of oil viscosity on drop dynamics in a vertical cell. In smooth cells, the velocity barely depends on  $\mu_o$  [Eq. (2)]. Conversely, in rough cells and below  $V_c$ , the velocity decreases as  $\mu_o$  increases, reflecting that viscous dissipation localizes inside the drop in the weakly lubricated regime. (c) Falling velocity in Hele-Shaw cells tilted by an angle  $\alpha$  with respect to the horizontal, for two configurations ( $e, \mu_o$ ): (1 mm, 1500 mPa.s) and (1.4 mm, 18000 mPa.s). A sharp velocity transition is also observed as  $\alpha$  exceeds a critical value. The drops smoothly fall even at the lowest inclinations ( $\alpha = 2.5^\circ$ ), highlighting the absence of pinning on the top of the pillars, which would result in a vanishing velocity at a finite value of  $\alpha$ .

Drops of fluorinated silicone oil (*poly(3,3,3)-trifluoropropylmethylsiloxane*, from Gelest) of volume  $\Omega$  and viscosity  $\mu_o$  ranging from 180 to 18000 mPa.s are inserted at the top of the cell. The interfacial tension between both liquids  $\gamma = 5\text{--}6$  mN/m (depending on the oil viscosity) is measured with the pendant drop method. As the oil density  $\rho_o = 1230\text{--}1250$  kg/m<sup>3</sup> is larger than the density of water ( $\rho_w = 997$  kg/m<sup>3</sup>), drops fall under gravity. This configuration ensures a controlled driving force, enabling a thorough characterization of the dissipation mechanisms [14,16]. As the surfactant solution completely wets the surface of the cell walls, no adhesion hinders the motion of the oil drops. The vertical trajectory of the drops is monitored with a digital camera.

The drops reach a constant velocity  $V$  after a few millimeters of descent. For fixed values of  $\mu_w$ ,  $\mu_o$ , and  $e$ ,  $V$  is independent of the volume within the limit of confined drops ( $R > e$ ). Because of the high contrast in viscosity between the drops and the surrounding solution, we expect  $V$  to markedly depend on the thickness  $b$  of the lubricating film, as shown by recent studies [14,16].

In a cell with *smooth* walls,  $b$  follows the classical Bretherton’s law [28]  $b \sim e/2\text{Ca}^{2/3}$ , for capillary numbers  $\text{Ca} = \mu_w V/\gamma$  ranging from  $10^{-5}$  to  $10^{-2}$ , as confirmed by recent experiments [11,17]. In this configuration, the dimensionless parameter  $m = \mu_w e/\mu_o b$  characterizes the efficiency of the lubrication process. For  $m \gg 1$ , the thin films of water cannot lubricate efficiently the motion. The flow in the volume of the drop thus follows a Poiseuille profile, which corresponds to the friction force  $F_f = 12\pi\mu_o VR^2/e$ . Balancing  $F_f$  with the apparent weight

of the “pancake” drop  $F_g = \pi(\rho_o - \rho_w)gR^2e$  leads to the sedimentation velocity

$$V = \frac{(\rho_o - \rho_w)g \sin \alpha}{12\mu_o} e^2. \quad (1)$$

However, in the present experimental conditions, the large inner-to-outer viscosity ratio ( $\mu_o/\mu_w > 180$ ) favors the opposite limit  $m \ll 1$ . In this regime, viscous drops tend to slide on the water films as solids. Viscous dissipation is now localized in the lubricating film, which results in the sublinear friction force  $F_f \sim \mu_w VR^2/b \sim \gamma R^2 \text{Ca}^{1/3}/e$  and leads to a strong dependence of the velocity on the gap,

$$V = \beta \frac{(\rho_o - \rho_w)^3 g^3 \sin^3 \alpha}{\mu_w \gamma^2} e^6, \quad (2)$$

where  $\beta = 4.3 \times 10^{-2}$  is determined experimentally in a previous work [16]. This regime, represented by open circles and full lines in Figs. 2(a) and 2(b) is hereafter called “strongly lubricated” and corresponds to velocities independent of the drop viscosity  $\mu_o$  (within the limit  $m \ll 1$ ).

In a cell with *rough* walls, the dynamics is dramatically altered, and the velocity is strongly reduced, as shown in Fig. 2. Although  $V$  displays a square dependence with  $e$ , its magnitude is about ten times larger than expected from a basic Poiseuille flow in the drop [Eq. (1) and dotted lines in Fig. 2]. We interpret this shift as a consequence of an effective slip due to the presence of water atop and between the pillars [19,21]. The origin of this “weakly lubricated” regime is discussed hereafter. Above a critical gap

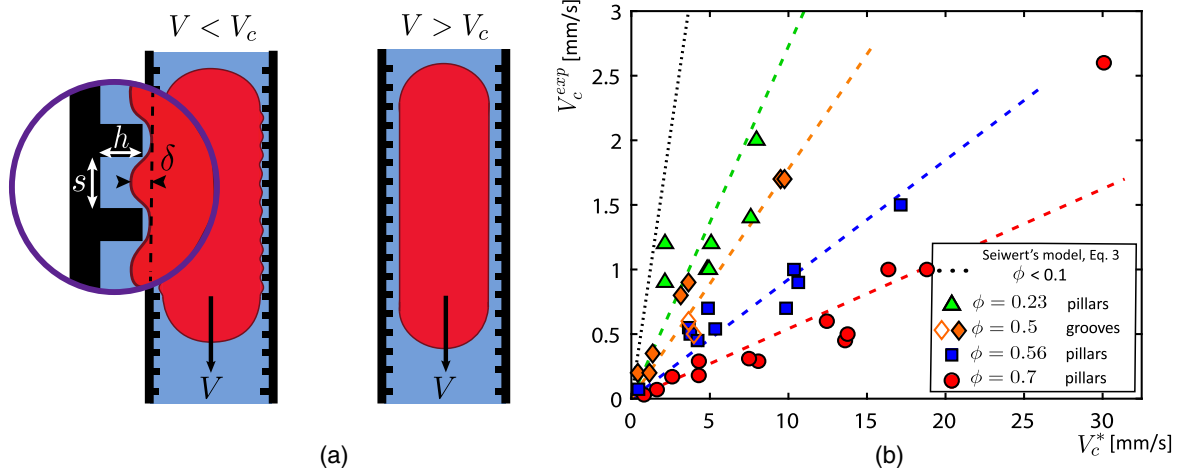


FIG. 3. (a) At small velocity ( $V < V_c$ ), the roughness-induced reduction of the viscous stress at the front meniscus of the drop hinders the deposition of a lubricating film. The drop is compressed in the pillars by the capillary pressure and its interface is corrugated. Furthermore, a thin nanometric film of water, stabilized by disjoining pressure, isolates the drop from the top of the pillars. Viscous dissipation localizes in the viscous drop, which strongly reduces its mobility. For  $V > V_c$ , the strong viscous stress at the front meniscus deforms the interface and allows the deposition of an efficient lubricating film. The dynamics of the case of smooth confinement is recovered. (b) Experimental critical velocity as a function of  $V_c^*$  [Eq. (3)], for different oil viscosities  $\mu_o$ , pillars heights  $h$ , and pillars densities and geometries:  $\phi = 0.23$  (green triangles, pillars),  $\phi = 0.50$  (full and open orange diamonds, grooves perpendicular and parallel to the trajectory of the droplets)  $\phi = 0.56$  (blue squares, pillars),  $\phi = 0.70$  (red circles, pillars). The large variations of  $V_c$  mainly originate from variations of  $h$ , ranging from 1.5 to 9  $\mu\text{m}$ . The variations of  $\mu_o$  from 180 to 18 000 mPa s only slightly alters  $V_c$ , due to the change of  $e_c$ , as shown in Fig. 2.

thickness  $e_c$ , corresponding to a critical speed  $V_c$ , we observe an abrupt jump in velocity, represented by arrows in Fig. 2 (see also movie 1, Supplemental Material [27]). For  $e > e_c$ , the sedimentation velocities match the velocities obtained in a smooth cell. The strongly lubricated regime is thus recovered and the velocity increases by more than 2 orders of magnitude at the jump. We carried out experiments with various texture heights  $h$  for a given pattern ( $w = 200 \mu\text{m}$ ,  $s = 25 \mu\text{m}$ ). Figure 2(a) illustrates that as  $h$  is increased from 1.5 to 9  $\mu\text{m}$ , the critical gap and critical velocity also increase. For the largest height ( $h = 9 \mu\text{m}$ ), the  $V_c$  is even not reached within the explored range of parameters. This spectacular effect is also observed for droplets of smaller viscosity, as plotted in Fig. 2(b). In the weakly lubricated regime ( $V < V_c$ ), the velocity of the drops increases as the oil viscosity  $\mu_o$  is decreased (from 18 000 to 1500 mPa s), which reflects that viscous dissipation localizes in the drop. For  $\mu_o = 1500 \text{ mPa s}$  (blue triangles) the velocity jump is also observed and for  $e > e_c$ , all velocities collapse on the same curve corresponding to the strongly lubricated regime [Eq. (2)]. The transition is also observed in cells of given thickness but tilted with respect to the horizontal with an angle  $\alpha$  [Fig. 2(c)]. At small  $\alpha$ , weakly lubricated drops move slowly but still smoothly, indicating the absence of pinning on the textures. Increasing effective gravity by tilting the cell, one recovers the sharp transition to the high velocity regime where drops do not feel the roughness. For a given texture pattern, the critical velocity  $V_c$  is the same

as the one measured in experiments where the gap has been varied.

The massive reduction of mobility of nonwetting drops with the wall roughness strongly contrasts with the common behavior of water confined in superhydrophobic channels, where the roughness-induced slippage at the walls promotes higher mobility in comparison with smooth walls [18–23]. We interpret this paradox as a consequence of the role of the surrounding fluid as a lubricant. Analogous results were observed by Seiwert *et al.* in a recent study on the coating of a textured plate removed from a bath of liquid [29]. Below a critical withdrawal velocity  $V_c$ , the liquid invades the textures (a dilute array of pillars), but the authors do not observe any coating above the height of the pillars. However, a coating film is deposited as the withdrawing velocity is increased above  $V_c$ . Applied to our configuration, this scenario leads to the two regimes sketched in Fig. 3(a). For  $V < V_c$ , the surrounding solution only fills the textures. The friction of the droplet on the textured walls is thus complex. Because of molecular interactions, a thin film of the solution may be present on the top of the pillars. The thickness of such a thin film is of the order of tens of nanometers [11,25,30], which limits its lubricating properties [16]. Furthermore, due to the strong confinement, Laplace pressure induces the formation of bumps between pillars of amplitude  $\delta \sim s^2/e \sim 500 \text{ nm}$ , which results in additional friction localized in the viscous drop [21,31]. The overall dissipation in this weakly lubricated regime should thus depend on

the topography of the texture and more specifically on the pillar density  $\phi = [w/(w+s)]^2$ . Describing in detail these processes would deserve a dedicated study and is beyond the scope of this Letter. In the opposite condition  $V > V_c$ , a lubricating layer of the solution covers the textures and dramatically reduces friction, as viscous dissipation localizes in the lubricating film of low viscosity. Modeling the impregnated textures as an effective viscous liquid layer in Bretherton's derivation, Seiwert *et al.* estimate the evolution of the deposited layer in their coating process [29]. As  $V$  is increased, the thickness quickly reaches the classical prediction from Bretherton [29] in agreement with the sudden jump observed in our experiments and with different derivations accounting for wall slip [32,33]. The transition between both regimes in the experiments of Seiwert is smooth: the thickness varies continuously with the imposed coating velocity. In contrast, our experiment is performed at a controlled driving force, which leads to a discontinuity in the velocity.  $V_c$  can be estimated as the velocity required to obtain a coating film of thickness  $h$  in a standard smooth situation [29]

$$V_c^* \sim \left( \frac{h}{e_c/2} \right)^{3/2} \frac{\gamma}{\mu_w}. \quad (3)$$

However, we also expect the pillar density  $\phi$  to play a major role in setting the transition. In Fig. 3(b), we plot the evolution of the critical velocity  $V_c^{\text{exp}}$  as a function of  $V_c^*$  for different values of  $\phi$ . Each set of measurements corresponds to different oil viscosities and pillar heights. Although experimental data display some scattering,  $V_c^{\text{exp}}$  is proportional to  $V_c^*$ , confirming the scaling. In addition, the prefactor is rather low for high values of  $\phi$  (of the order of 0.05 for  $\phi = 0.7$ ). In the limit  $\phi \rightarrow 1$ , corresponding to smooth walls, we expect  $V_c^{\text{exp}}$  to vanish. Conversely, the prefactor approaches unity as  $\phi$  decreases. The result from Seiwert *et al.*, represented with a dotted line was experimentally obtained within the limit  $\phi < 0.1$  [29].  $V_c^*$  is inversely proportional to  $\mu_w$ , meaning that increasing the outer viscosity favors the abrupt velocity jump. This dependence leads to counter-intuitive results when viscous glycerol is added to the outer aqueous solution (50% in volume of glycerol, as detailed in the Supplemental Material [27]). In Fig. 4 we compare the falling velocity of droplets in solutions of viscosity  $\mu_w = 1$  and 8 mPa s. In the case of smooth surfaces, the droplets move faster in the solution of lower viscosity, in agreement with Eq. (2) and common intuition. However, the case of rough surfaces is more surprising. For high confinement, the velocity is low and does not display a strong dependence on  $\mu_w$ . The jump appears first with the viscous solution, leading to a sharp increase of the velocity as expected from Eq. (3). Within a certain range of confinement (green region in Fig. 4), droplets move faster when surrounded by a more viscous solution (Supplemental Material [27], movie 2). Provided

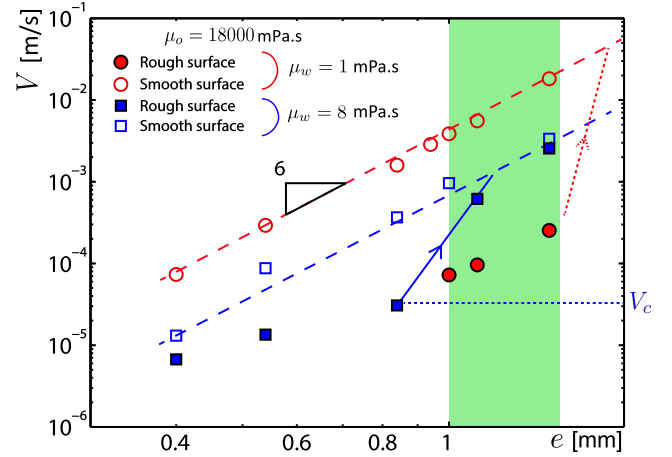


FIG. 4.  $V$  vs  $e$  for drops of  $\mu_o = 18000$  mPa s in smooth and rough confinements (open and full symbols, respectively). The blue squares correspond to droplets advancing in vertical cells filled with a viscous water-glycerol mixture ( $\mu_w = 8$  mPa s), the red circles to droplets in cells filled with water ( $\mu_w = 1$  mPa s) inclined by  $30^\circ$  with respect to the horizontal. This inclination compensates for the change of density  $\rho_w$  of the aqueous solution upon addition of dense glycerol and guarantees a similar driving force between both experiments (see Supplemental Material [27] for details). In the green-colored region, much larger velocities are counterintuitively obtained for drops evolving in a more viscous environment ( $\mu_w = 8$  mPa s, see also Supplemental Material [27], movie 2). The red dashed arrow represents the velocity jump expected if larger gaps  $e$  could be tested.

higher gap thicknesses could be tested, one would also expect the data for  $\mu_w = 1$  mPa s to exhibit an abrupt velocity jump (dashed arrows in Fig. 4), and the intuitive behavior would be restored: the more viscous the outer phase, the slower the drops.

This Letter illustrates the intricate dissipation mechanisms acting at the vicinity of rough surfaces. Below a critical velocity, roughness decreases the friction at the front meniscus of the drop. As an illustration, we show in the Supplemental Material [27] that buoyant confined air bubbles tend to rise faster in textured Hele-Shaw cells than between smooth walls. In this configuration, the outer fluid is more viscous than the inner air and the motion is mainly resisted by friction in the vicinity of the peripheral menisci [34,35]. The higher mobility observed at small Ca highlights the role of roughness in reducing friction in these menisci. In the case of viscous drops, the impact of roughness is dramatically different. The reduced viscous friction at the front meniscus of the drop hinders the deformation of the interface and the formation of an efficient lubricating film. This results in a corrugated interface [Fig. 3(a)] and in the localization of dissipation in the viscous drop. We finally showed that by increasing the viscosity of the outer fluid, the viscous friction at the periphery is increased and a thick lubricating layer is restored, therefore leading to faster drops.

Depending on the inner-to-outer viscosity ratio  $\mu_o/\mu_w$ , we showed that the apparent roughness-induced reduction of friction in the vicinity of the meniscus can accelerate air bubbles or, as a paradox, substantially slow down highly viscous droplets. A direct observation of the structure of the lubricating film would enable one to accurately describe the configurations qualitatively represented in Fig 3(a), using, for instance, Reflection Interference Contrast Microscopy (RICM) [11,17] or confocal microscopy [36].

The results of our sedimentation experiment fully apply to drops entrained by a surrounding fluid in a confined environment, such as microfluidic channels [7,8] or porous media [6]. In practice, controlling the friction of viscous droplets through a designed texture might constitute an efficient tool to probe the rheological properties of droplets, vesicles or biological cells, and possibly achieve specific sorting.

The authors thank K. Jaafar for his initial contribution to the project. They also acknowledge funding from Total S.A. and support from Institut Pierre-Gilles de Gennes, “Investissements d’avenir,” program ANR-10-EQPX-34.

\*ludovic.keiser@espci.org

†etienne.reyssat@espci.fr

- [1] T. C. Ransohoff, P. A. Gauglitz, and C. J. Radke, Snap-off of gas bubbles in smoothly constricted noncircular capillaries, *AIChE J.* **33**, 753 (1987).
- [2] P. G. Saffman and G. I. Taylor, The penetration of a fluid into a porous medium or Hele-Shaw cell containing a more viscous liquid, *Proc. R. Soc. A* **245**, 312 (1958).
- [3] T. T. Al-Housseiny, P. A. Tsai, and H. A. Stone, Control of interfacial instabilities using flow geometry, *Nat. Phys.* **8**, 747 (2012).
- [4] C. Odier, B. Levaché, E. Santanach-Carreras, and D. Bartolo, Forced Imbibition in Porous Media: A Fourfold Scenario, *Phys. Rev. Lett.* **119**, 208005 (2017).
- [5] L. Keiser, R. Herbaut, J. Bico, and É. Reyssat, Washing wedges: Capillary instability in a gradient of confinement, *J. Fluid Mech.* **790**, 619 (2016).
- [6] A. Z. Zinchenko and R. H. Davis, Motion of deformable drops through porous media, *Annu. Rev. Fluid Mech.* **49**, 71 (2017).
- [7] C. Baroud, F. Gallaire, and R. Dangla, Dynamics of microfluidic droplets, *Lab Chip* **10**, 2032 (2010).
- [8] R. Seemann, M. Brinkmann, T. Pfohl, and S. Herminghaus, Droplet based microfluidics, *Rep. Prog. Phys.* **75**, 016601 (2012).
- [9] A. de Lózar, A. L. Hazel, and A. Juel, Scaling Properties of Coating Flows in Rectangular Channels, *Phys. Rev. Lett.* **99**, 234501 (2007).
- [10] S. Jakiela, P. M. Korczyk, S. Makulska, O. Cybulski, and P. Garstecki, Discontinuous Transition in a Laminar Fluid Flow: A Change of Flow Topology Inside a Droplet Moving in a Micron-Size Channel, *Phys. Rev. Lett.* **108**, 134501 (2012).
- [11] A. Huerre, O. Théodoly, A. M. Leshansky, M.-P. Vagnat, I. Cantat, and M.-C. Jullien, Droplets in Microchannels: Dynamical Properties of the Lubrication Film, *Phys. Rev. Lett.* **115**, 064501 (2015).
- [12] L. Zhu and F. Gallaire, A pancake droplet translating in a Hele-Shaw cell: Lubrication film and flow field, *J. Fluid Mech.* **798**, 955 (2016).
- [13] Y. Ling, J.-M. Fullana, S. Popinet, and C. Josserand, Droplet migration in a Hele-Shaw cell: Effect of the lubrication film on the droplet dynamics, *Phys. Fluids* **28**, 062001 (2016).
- [14] M. Yahashi, N. Kimoto, and K. Okumura, Scaling crossover in thin-film drag dynamics of fluid drops in the Hele-Shaw cell, *Sci. Rep.* **6**, 31395 (2016).
- [15] G. Balestra, L. Zhu, and F. Gallaire, A viscous droplet in a capillary tube: From Bretherton’s theory to empirical models, *Microfluid. Nanofluid.* **22**, 67 (2018).
- [16] L. Keiser, K. Jaafar, J. Bico, and É. Reyssat, Dynamics of non-wetting drops confined in a Hele-Shaw cell, *J. Fluid Mech.* **845**, 245 (2018).
- [17] B. Reichert, A. Huerre, O. Théodoly, M.-P. Vagnat, I. Cantat, and M.-C. Jullien, Topography of the lubrication film under a pancake droplet traveling in a Hele-Shaw cell, *J. Fluid Mech.* **850**, 708 (2018).
- [18] O. I. Vinogradova, Slippage of water over hydrophobic surfaces, *Int. J. Miner. Process.* **56**, 31 (1999).
- [19] É. Lauga and H. A. Stone, Effective slip in pressure-driven Stokes flow, *J. Fluid Mech.* **489**, 55 (2003).
- [20] C.-H. Choi and C.-J. Kim, Large Slip of Aqueous Liquid Flow over a Nanoengineered Superhydrophobic Surface, *Phys. Rev. Lett.* **96**, 066001 (2006).
- [21] C. Ybert, C. Barentin, C. Cottin-Bizonne, P. Joseph, and L. Bocquet, Achieving large slip with superhydrophobic surfaces: Scaling laws for generic geometries, *Phys. Fluids* **19**, 123601 (2007).
- [22] J. P. Rothstein, Slip on superhydrophobic surfaces, *Annu. Rev. Fluid Mech.* **42**, 89 (2010).
- [23] D. Schäffel, K. Koynov, D. Vollmer, H. J. Butt, and C. Schönecker, Local Flow Field and Slip Length of Superhydrophobic Surfaces, *Phys. Rev. Lett.* **116**, 134501 (2016).
- [24] J. D. Smith, R. Dhiman, S. Anand, E. Reza-Garduno, R. E. Cohen, G. H. McKinley, and K. K. Varanasi, Droplet mobility on lubricant-impregnated surfaces, *Soft Matter* **9**, 1772 (2013).
- [25] D. Daniel, J. Timonen, R. Li, S. Velling, and J. Aizenberg, Oleoplaning droplets on lubricated surfaces, *Nat. Phys.* **13**, 1020 (2017).
- [26] A. Keiser, L. Keiser, C. Clanet, and D. Quéré, Drop friction on liquid-infused materials, *Soft Matter* **13**, 6981 (2017).
- [27] See Supplemental Material at <http://link.aps.org/supplemental/10.1103/PhysRevLett.122.074501>, for the description of the movies, details on experimental methods, and additional experimental results on the gravity-driven motion of bubbles confined between textured walls.
- [28] F. P. Bretherton, The motion of long bubbles in tubes, *J. Fluid Mech.* **10**, 166 (1961).
- [29] J. Seiwert, C. Clanet, and D. Quéré, Coating of a textured solid, *J. Fluid Mech.* **669**, 55 (2011).
- [30] J. N. Israelachvili, *Intermolecular and Surface Forces*, 3rd ed. (Elsevier, New York, 2011).

- [31] D. Einzel, P. Panzer, and M. Liu, Boundary Condition for Fluid Flow: Curved or Rough Surfaces, *Phys. Rev. Lett.* **64**, 2269 (1990).
- [32] Y.-C. Liao, Y.-C. Li, and H.-H. Wei, Drastic Changes in Interfacial Hydrodynamics due to Wall Slippage: Slip-Intensified Film Thinning, Drop Spreading, and Capillary Instability, *Phys. Rev. Lett.* **111**, 136001 (2013).
- [33] Y.-C. Li, Y.-C. Liao, T.-C. Wen, and H.-H. Wei, Breakdown of the Bretherton law due to wall slippage, *J. Fluid Mech.* **741**, 200 (2014).
- [34] I. Cantat, Liquid meniscus friction on a wet plate: Bubbles, lamellae, and foams, *Phys. Fluids* **25**, 031303 (2013).
- [35] É. Reyssat, Drops and bubbles in wedges, *J. Fluid Mech.* **748**, 641 (2014).
- [36] F. Schellenberger, J. Xie, N. Encinas, A. Hardy, M. Klapper, P. Papadopoulos, H.-J. Butt, and D. Vollmer, Direct observation of drops on slippery lubricant-infused surfaces, *Soft Matter* **11**, 7617 (2015).